Version October 15, 2026
Preprint typeset using LaTeX style openjournal v. 09/06/15

arXiv:2610.19838v1 [astro-ph.GA] 14 Oct 2026

A HETEROGENEOUS SET OF UNUSUAL QUASARS SELECTED FROM ASTROMETRY AND BROAD-BAND PHOTOMETRY

C. Cheng[1,2], K. Valeckas[1,2,3,4], L. Christensen[1,2], A. Henderson de la Fuente[3,5], L. Fuglsang[2,3,6], V. Vuolteenaho[3,7], N. Pyykkinen[3,8], R. H. Rasmussen[3,9], S. Bijavara Seshashayana[3,10], J. P. U. Fynbo[1,2*]

[1]Cosmic DAWN Center
[2]Niels Bohr Institute, Copenhagen University, Jagtvej 155, DK-2200 Copenhagen N, Denmark
[3]Nordic Optical Telescope, Rambla José Ana Fernández Pérez 7, ES-38711 Brēna Baja, Spain
[4]European Southern Observatory, Alonso de Córdova 3107, Vitacura, Región Metropolitana, Chile
[5]Department of Physics, University of Oxford, Keble Road, Oxford, OX1 3RH, UK
[6]Centre de Recherche Astrophysique de Lyon, Université Lyon 1, 9 Avenue Charles André, 69561 Saint Genis Laval, France
[7]Space Physics and Astronomy Research Unit, University of Oulu, P.O. Box 3000, FI-90014 University of Oulu, Finland
[8]Department of Physics and Astronomy, University of Turku, FI20014 Turku, Finland
[9]Department of Physics and Astronomy, Aarhus University, Ny Munkegade 120, DK-8000, Aarhus C, Denmark and
[10]Materials Science and Applied Mathematics, Malmö University, SE-205 06 Malmö, Sweden

Version October 15, 2026

ABSTRACT

The aim of this study is to explore methods for how to identify new quasars with different properties with regard to reddening, redshift, the presence of broad absorption lines from outflows, or other rare properties affecting the broad-band colours. We use Gaia-based astrometric pre-selection to study only sources that have zero parallax and zero proper motion within errors. We subsequently match these sources with information from wide-area photometric surveys and build colour-colour diagrams. Based on these diagrams we select targets for follow-up spectroscopy. In the subsequent analysis we also apply observations from SPHEREx to firmly establish redshifts. We secure spectroscopic observations for 24 sources. Of these, three are found to be stars and the remaining 21 are classified as quasars spanning a redshift range from $z = 0.139$ to $z = 3.732$. The majority of the sources located away from the normal quasar locus in colour-colour diagrams are found to be broad-absorption-line quasars. A single source, the lowest redshift source at $z = 0.139$, is reminiscent of the so-called Little Red Dots found at high redshifts with JWST. Using the simple procedure followed here it is possible to locate previously undiscovered quasars with interesting properties, in particular Broad Absorption Line quasars and quasars with unusual extinction.

1. INTRODUCTION

Since their discovery in the 1960s, quasars have played a central role in extragalactic astronomy, serving as powerful probes of the early Universe and as tracers of accretion onto supermassive black holes at the centres of galaxies (Fan 2006). Powered by accretion onto supermassive black holes (Rees 1984), quasars provide key insights into the physics of active galactic nuclei (AGN), the growth of supermassive black holes, and their interplay with galaxy evolution, as well as the properties of the intervening intergalactic medium (Rees 1984; Hopkins et al. 2006; Meiksin 2009).

Historically, quasars have been identified using a variety of selection techniques. Early surveys primarily relied on radio emission, leading to the discovery of the first quasar samples (Schmidt 1963). While radio selection is largely insensitive to dust extinction, it is intrinsically biased towards the radio-loud population, which represents only a small fraction of the overall quasar population (Sandage 1965). Hence it was realized that radio-selection alone cannot provide a complete census of quasars.

Subsequently, colour-based selection methods became the dominant approach, particularly with the advent of wide-area optical surveys. By exploiting the distinctive colours of quasars relative to stars, optical selection has enabled the construction of large quasar catalogs with up to a million sources. Extensions to the near- and mid-infrared have further improved selection efficiency and helped recover quasars missed in optical surveys. However, all colour-based techniques ultimately depend on the observed spectral energy distributions of sources and therefore remain susceptible to colour-dependent biases, especially for quasars affected by dust reddening or strong absorption features such as Broad Absorption Lines (BALs, Gibson et al. 2009).

An alternative and complementary approach to quasar selection is provided by astrometric methods (e.g., Koo et al. 1986; Meusinger et al. 2002). This approach exploits the negligible parallax and proper motion of quasars, e.g. using very precise observations from the Gaia mission (Gaia Collaboration et al. 2016), to identify candidates independently of their spectral energy distributions or colours. Previous studies have demonstrated the feasibility of this approach using both simulated and real Gaia data, confirming that astrometric

* Corresponding author. jfynbo@nbi.ku.dk

selection can recover quasars that are underrepresented in traditional colour-based samples (Heintz et al. 2015, 2018, 2020; Geier et al. 2019; Fynbo et al. 2020).

In this work, we use a criterion of zero proper motion and a parallax of zero as an astrometric pre-selection and sample sources from different regions of colour–colour space to investigate the connection between photometric properties and spectroscopic characteristics. This selection is not optimized for completeness or sample purity, but is instead designed to explore the diversity of spectroscopic characteristics among astrometrically selected candidates.

The paper is organized in the following way: In Sect. 2 we describe how the targets of this study have been selected. In Sect. 3 we describe the observations, which mostly come from a summer school in August 2024, with additional observations extending the sample in 2025. In Sect. 4 we describe our results, which mainly consists of analysis of the spectra and classification of the sources in terms of object class (star or quasar, which type of quasar), extinction and redshift. In Sect. 5 we discuss the implications of our work and in Sect. 6 we provide our conclusions.

2. SELECTION STRATEGY

The target selection in this work was designed to investigate the spectroscopic properties of quasar candidates occupying different regions of colour–colour space. Without the inclusion of astrometric information such a study is nearly impossible as some regions of colour-space are swamped by stellar sources making it very difficult to pick out the rare non-stellar sources in these regions of colr-space. We have adopted a selection strategy that combines an astrometric pre-selection, and hence rejection of the large majority of stellar sources, with targeted sampling based on photometric properties.

2.1. *Astrometric pre-selection*

We first selected sources from the Gaia catalogue with proper motions and parallaxes consistent with zero within the measurement uncertainties. Such sources are expected to be dominated by extragalactic objects and therefore constitute a natural pool of quasar candidates. Our SQL-query for the astrometric preselection is provided in Fig. 1. This set of objects we will refer to as our master catalogue.

2.2. *Further down-selection based on position in colour–colour space*

These astrometrically selected sources were then cross-matched with photometric data from the Sloan Digital Sky Survey (SDSS, bands u, g, r, i, z, Alam et al. 2015), as well as complementary near- and mid-infrared data from the Two Micron All Sky Survey (2MASS, bands J, H, K, Skrutskie et al. 2006) and the Wide-field Infrared Survey Explorer (WISE, bands $W1, W2, W3, W4$, Wright et al. 2010).

Using the available photometry, we constructed colour–colour diagrams for further down-selection of targets for spectroscopic follow-up. We use two main colour-colour diagrams, namely $g-r$ versus $J-K$ and $W1-W2$ vs. $J-K$. These diagrams provide very useful separations of stars, galaxies and quasars (e.g., Fynbo et al. 2017; Geier et al. 2019). In colour–colour space, the expected distributions of stars and quasars can be understood from theoretical templates. As illustrated in Figure 2, stars follow a narrow and well-defined track in the $g-r$ versus $J-K$ diagram, reflecting the relatively uniform spectral energy distributions of stellar populations. In contrast, quasars do not occupy a single linear sequence but instead populate a broader and more structured locus with a finite width due to redshift, which moves the strong emission lines in and out of the various filters and removes light due to Lyman-α forest blanketing at $z \gtrsim 2.5$, and different levels of extinction. In particular, the position of the Hα line to a large extent explains the spread in $J-K$ colour for quasars.

```
SELECT TOP 50000000
    source_id, ra, dec, l, b,
    pmra, pmra_error,
    pmdec, pmdec_error,
    parallax, parallax_error,
    phot_g_mean_mag,
    phot_g_mean_flux,
    phot_g_mean_flux_error,
    phot_bp_mean_mag,
    phot_rp_mean_mag,
    bp_rp,
    ref_epoch
FROM gaiaedr3.gaia_source AS gaia
WHERE
    gaia.ra >= 270
    AND gaia.ra <= 359
    AND gaia.dec > 0
    AND gaia.phot_g_mean_mag <= 19
    AND ABS(gaia.parallax/gaia.parallax_error) <= 2
    AND (
        POWER(gaia.pmra/gaia.pmra_error,2)
      + POWER(gaia.pmdec/gaia.pmdec_error,2)
    ) <= 4
```

FIG. 1.— The SQL query we have used to pre-select stationary and distant Gaia EDR3 sources for this mini-survey.

Although the stellar and quasar loci are largely separated, Fig. 2 also shows that partial overlap is expected in specific regions of colour–colour space. On the left side of the $g-r$ vs. $J-K$ diagram, at relatively blue near-infrared colours ($J-K \lesssim 0.6$), the stellar locus forms a comparatively clean and "safe" region dominated by stars. At larger $J-K$ values, stellar templates continue to appear but increasingly overlap with the quasar locus, particularly with blue quasar tracks. For quasars, a relatively safe region is found in the lower part of the quasar locus, where little overlap with the stellar sequence is expected. In the $W1-W2$ vs. $J-K$ diagram there is also overlap between different classes of objects at $W1-W2 \approx 0.5$. These theoretical predictions indicate that although much of colour–colour space allows fairly robust source classification, certain transition regions are more ambiguous.

Targets were selected from different regions of these diagrams for spectroscopic follow-up, including both regions where stars and quasars are well separated and regions where their distributions overlap.

Rather than optimizing the selection for sample purity or completeness, this approach was adopted to probe the diversity of spectroscopic properties associated with different locations in colour–colour space. By sampling both photometrically "clean" regions and more ambiguous transitional regions, this strategy allows a direct as-

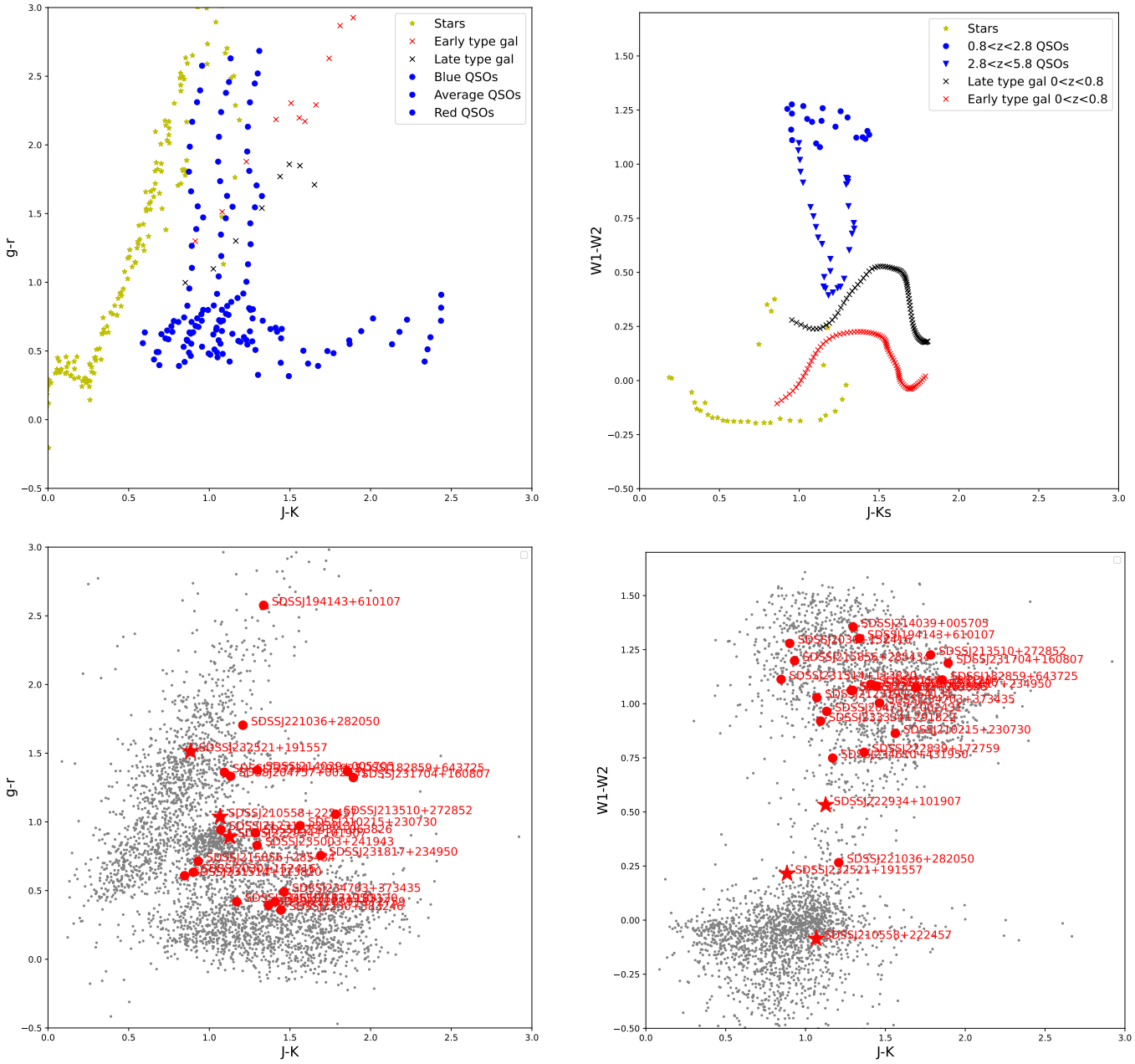


FIG. 2.— Colour–colour diagrams. *Top panels:* Theoretical colour-tracks for stars, galaxies and quasars. *Top Left:* Colours derived using the templates from Hewett et al. (2006) as described in Fynbo et al. (2017). *Top Right:* For this diagram we calculate synthetic colours using templates from Assef et al. (2010); Husser et al. (2013); Selsing et al. (2016). *Bottom panels:* colours of objects in the master catalogue. Confirmed quasars are shown with filled circles and stars with an asterisk.

sessment of the extent to which photometric location reflects the properties such as redshift, extinction and the presence of BAL features of the sources.

3. OBSERVATIONS

All spectroscopic observations presented in this work were made with the 2.56-m NOT located on the Canarian island of La Palma, using the Andalucia Faint Object Spectrograph and Camera (ALFOSC). ALFOSC was chosen for its efficiency in observing faint sources, making it well suited for low- to intermediate-resolution long-slit spectroscopy of quasar candidates.

Most targets were observed using grism 4, which provides a wavelength coverage of approximately 3200–9600 Å with a spectral resolution of slightly below 400 when using a 1" slit. This setup is well suited for identifying prominent emission and absorption features in quasar spectra over a wide redshift range. A subset of targets was re-observed using grism 20, covering the wavelength range 5650–10150 Å, to obtain follow-up spectra with improved sensitivity at longer wavelengths and approximately double the resolution compared to grism 4. Both grism 4 and grism 20 suffer from about 5% 2nd-order contamination redward of 9000 Å. This combination of grisms offers broad wavelength coverage while maintaining a suitable balance between spectral resolution and signal-to-noise ratio for reliable spectral classifi-

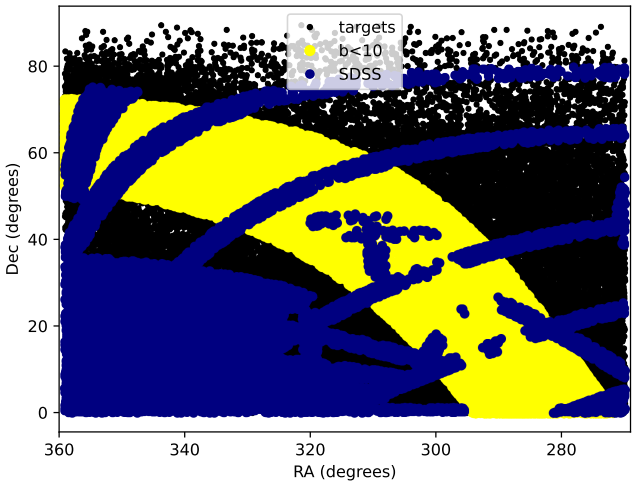


FIG. 3.— Our targets are selected to be observable from La Palma in August. Targets are selected to be above a Galactic height of 10 degrees and from the parts of the northern summer sky covered by SDSS. For these regions there is also available photometry from 2MASS and WISE.

cation and redshift determination. A complete list of the observed targets, together with their coordinates and observational parameters, is provided in Table 1 and Table 2.

The spectroscopic data were reduced using standard procedures for long-slit spectroscopy, including bias subtraction, flat-field correction, wavelength calibration, sky subtraction, spectral extraction, and flux calibration. Data reduction and analysis were performed using Python-based routines as implemented in the Python-package PyLongslit (Valeckas et al. 2025), which is available on Github[2].

4. RESULTS

4.1. *Spectroscopic classification*

Spectroscopic observations were obtained for 24 candidates. Based on the inspection of the one-dimensional spectra and comparison with quasar templates, 21 objects are confirmed as quasars, the remaining 3 targets are classified as stellar contaminants. To classify the objects we plot the optical spectra from our own observations together with photometry from SDSS; UKIDSS, and WISE and with spectroscopic data from SPHEREx (Bock et al. 2026). The SPHEREx spectra are acquired using the SPHEREx pipeline available on Github[3]. WISE photometry is in particular interesting as the The criterion $W1-W2>0.8$ is a robust selector for quasars at $z<2.8$ (Stern et al. 2012). At higher redshifts $W1-W2$ drops and blends with the $W1-W2$ colours of stars and galaxies (see Fig. 2).

For quasar candidates, redshifts and dust extinction values were estimated by comparing the observed spectra with a representative quasar template, for which we adopt the Selsing et al. (2016) quasar template, reddened using an SMC-like extinction curve as quantified by Pei (1992). For BAL quasars, where emission lines may be strongly suppressed, redshift determinations primarily rely on absorption features and on emission lines in the SPHEREx spectral region (Hα in particular).

We also cross-check with the FIRST and LOFAR survey for emission at radio wavelengths (Helfand et al. 2015; de Gasperin et al. 2023).

The classifications of all targets, together with the estimated redshifts and extinction values, are listed in Table 3. Fig. 2 shows the positions of all targets in the $g-r$ versus $J-K$ diagram, with the spectroscopic classifications indicated by different symbols and the redshifts represented by colour.

4.2. *Notes on individual objects*

The position of the objects in the colour-colour diagrams can be inspected in Fig. 2

4.2.1. *SDSS J182859+643725 ($z=0.609$)*

This object has colours $g-r=1.37$, $J-K=1.86$, and $W1-W2=1.11$. It was selected due to its red optical and near-infrared colours. For this quasar we identify a redshift of $z=0.609$, determined based on a prominent broad emission feature near 7800 Å, which is interpreted as Hβ (Fig. 4). This redshift is consistent with the SPHEREx spectrum, which shows very strong Hydrogen emission lines consistent with this redshift (Hα, Pα, Pβ). The SPHEREx spectrum has the wrong continuum shape compared to the photometry, which is due to contamination of emission from another brighter source within the SPHEREx PSF. A dust extinction value of $A_V=1.4$ is estimated, as it yields a good match between the photometric data and the quasar template in the near-infrared region. This dust extinction value shows that the quasar spectrum is heavily reddened by dust.

There is a strong absorption trough on the red side of the Hβ emission, above what can be accounted for by telluric absorption at these observed wavelengths, which we have not been able to identify. One possibility is He I. There is also evidence for blueshifted Hβ absorption, but this is blended with the telluric A band. There is also blueshifted Mg II absorption.

At shorter wavelengths, the observed spectrum falls well below the reddened template. This discrepancy may indicate that the actual dust extinction curve is steeper in the UV than the adopted SMC-like law, which is discussed in Fynbo et al. (2013). Due to the peculiar nature of this spectrum, a second observation was carried out using grism 20, which extends the wavelength coverage toward longer wavelengths. The result from this second observation is consistent with the grism 4 spectrum in the overlapping region, confirming the reliability of the earlier data. In the newly covered longer-wavelength range, abroad absorption feature is observed just before Hα, which supports the classification of this object as a peculiar BAL quasar. We subsequently realized that this quasar is also observed as part of BOSS, but as far as we can see the redshift has not been established prior to our study. The source is detected by LOFAR with a flux of 8.20±0.08 mJy.

4.2.2. *SDSS J194143+610107 ($z=1.042$)*

This object has colours $g-r=2.58$, $J-K=1.34$, and $W1-W2=1.30$. It was selected for follow-up spectroscopy due to its very red optical colour (the red-

[2] https://kostasvaleckas.github.io/PyLongslit/index.html
[3] https://github.com/andrijazupic/SPHEREx_pipeline/tree/main

TABLE 1
ALL TARGETS OBSERVED WITH GRISM 4.

Target	RA (J2000) *[hr:min:sec]*	Dec (J2000) *[deg:min:sec]*	Date	Exposure Time *[s]*	Airmass
SDSS J182859+643725	18:28:59.34	+64:37:25.30	2024-08-10	2×300	1.34
SDSS J194143+610107	19:41:43.66	+61:01:07.80	2024-08-05	2×300	1.22
SDSS J203008+152416	20:30:08.82	+15:24:16.00	2024-08-05	2×300	1.30
SDSS J204757+002431	20:47:57.18	+00:24:31.50	2024-08-10	2×500	1.14
SDSS J210215+230730	21:02:15.48	+23:07:30.72	2025-07-31	2×600	1.01
SDSS J210558+222457	21:05:58.53	+22:24:57.00	2024-08-07	2×300	1.06
SDSS J212319+254131	21:23:19.53	+25:41:31.20	2024-08-10	2×300	1.02
SDSS J213510+272852	21:35:10.10	+27:28:52.20	2024-08-09	2×400	1.21
SDSS J214039+005705	21:40:39.85	+00:57:05.80	2024-08-10	2×300	1.13
SDSS J215731+183120	21:57:31.94	+18:31:20.40	2024-08-09	2×200	1.02
SDSS J215856+285434	21:58:56.42	+28:54:34.50	2024-08-06	2×300	1.00
SDSS J221036+282050	22:10:36.32	+28:20:50.65	2025-08-11	2×1200	1.06
SDSS J222839+172759	22:28:39.76	+17:27:59.57	2025-07-18	2×600	1.02
SDSS J222943+101907	22:29:34.34	+10:19:07.99	2024-08-09	2×300	1.20
SDSS J223052+383246	22:30:22.53	+38:32:46.60	2024-08-09	2×300	1.09
SDSS J225432+063826	22:54:32.27	+06:38:26.04	2025-08-22	2×900	1.08
SDSS J231514+113820	23:15:14.30	+11:38:20.20	2024-08-24	2×600	1.05
SDSS J231704+160807	23:17:04.31	+16:08:07.30	2024-08-09	2×300	1.14
SDSS J231817+234950	23:18:17.92	+23:49:50.10	2025-08-22	2×1200	1.20
SDSS J232521+191557	23:25:21.01	+19:15:57.06	2024-08-10	2×300	1.10
SDSS J233334+291822	23:33:34.32	+29:18:22.08	2025-09-20	2×1400	1.29
SDSS J234610+431950	23:46:10.77	+43:19:50.61	2024-08-09	2×300	1.06
SDSS J234703+373435	23:47:03.04	+37:34:35.10	2024-08-25	2×900	1.15
SDSS J235003+241943	23:50:03.81	+24:19:43.79	2025-07-30	2×900	1.02

TABLE 2
ALL TARGETS OBSERVED WITH GRISM 20.

Target	RA (J2000) *[hr:min:sec]*	Dec (J2000) *[deg:min:sec]*	Date	Exposure Time *[s]*	Airmass
SDSS J231704+160820	23:17:04.31	+16:08:20.70	2024-08-25	2×600	1.02
SDSS J182859+643725	18:28:59.34	+64:37:25.30	2024-08-10	2×500	1.32
SDSS J204757+002034	20:47:57.18	+00:20:34.50	2024-09-05	2×600	1.15

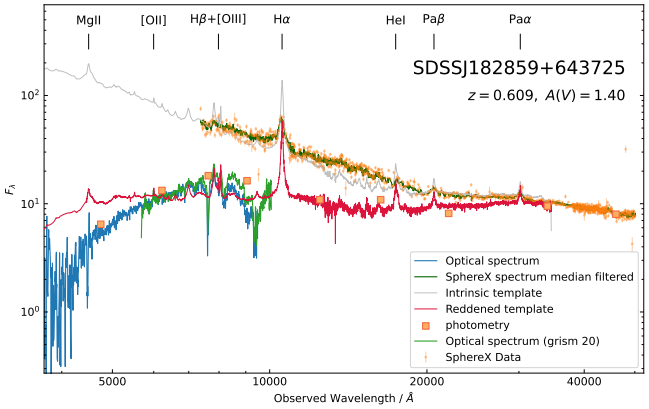


FIG. 4.— The spectrum of SDSS J182859+643725. All figures of individual quasar spectra has this layout: in blue (grism 4) and green (grism 20 when available) we show our optical spectra. The SPHEREx spectra are shown with orange (individual points) and green (median filtered). The photometry from SDSS, 2MASS, and WISE is shown with orange squares. The quasar template is shown in grey (unreddened) and red (reddened with an SMC extinction curve). The redshift and the assumed A_V is indicated on the figure. We classify this source as a peculiar BAL quasar. The SPHEREx spectrum is blended with light from a brighter source.

dest in the sample). This quasar spectrum (Fig. 5) exhibits a heavily suppressed continuum, with no prominent $z = 1.042$ based on the identification of several strong absorption lines, including Fe IIλ3301,λ3363 and CaII(λ3934,λ3969). At this redshift other absorption features align well with some low-ionization transitions such as Ti II and Mg I. The quasar shows broad and deep absorption troughs across the 6000 to 8500 Å range, and many absorption features are blended, forming a complex profile. The dust extinction is estimated to be $A_V = 1.4$, which gives a good match between the template and the photometric data in the NIR. In the SPHEREx spectrum there are emission lines consistent with Paα and Hα at the proposed redshift. The SPHEREx spectrum is contaminated by another bright source at the edge of the SPHEREx PSF, which explains why the slope does not match the photometry. The combination of multiple low-ionization metal lines (e.g., Fe II, Mg I, Ti II), suppressed UV emission lines, strong continuum depression, and wide absorption features lead us to classify this object as a FeLoBAL quasar. We subsequently realised that this object has also been observed as part of BOSS, but as far as we can see the redshift has not been established prior to our study. The source is detected by

TABLE 3
QUASAR SAMPLE: CLASSIFICATION, REDSHIFT AND EXTINCTION.

Target	Type	Redshift	A_V
SDSS J182859+643725	peculiar/BAL	0.609	1.4
SDSS J194143+610107	BAL	1.042	1.4
SDSS J203008+152416	BAL	1.741	0.0
SDSS J204757+002431	BAL	1.85	0.80
SDSS J210215+230730	normal	0.139	?
SDSS J210558+222457	star	0.0	0.0
SDSS J212319+254131	BAL	2.520	0.1
SDSS J213510+272852	BAL	2.43	0.20
SDSS J214039+005705	peculiar	1.1555	0.55
SDSS J215731+183120	normal	2.02	0.15
SDSS J215856+285434	BAL	1.553	0.0
SDSS J221036+282050	normal	3.732	0.2
SDSS J222839+172759	BAL	2.932	0.25
SDSS J222934+101907	star	0.0	0.0
SDSS J223030+383246	normal	2.26	0.0
SDSS J225432+063826	peculiar	2.698	0.40
SDSS J231514+113820	BAL	2.895	0.2
SDSS J231704+160807	peculiar	0.464	1.7
SDSS J231817+234950	normal	0.570	1.50
SDSS J232521+191557	star	0.0	0.0
SDSS J233334+291822	BAL	1.675	0.60
SDSS J234610+431950	normal	3.26	0.0
SDSS J234703+373435	normal	3.03	0.20
SDSS J235003+241943	peculiar	0.692	0.3

LOFAR with a flux of 2.23±0.12 mJy.

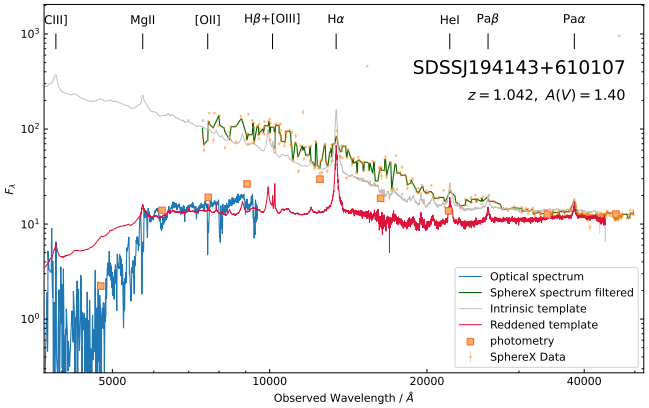


FIG. 5.— The spectrum of SDSS J194143+610107. We classify this source as a FeLoBAL quasar. The SPHEREx spectrum is blended with light from a brighter source.

4.2.3. *SDSS J203008+15241616 ($z = 1.741$)*

This object has colours $g - r = 0.631$, $J - K = 0.90$, and $W1 - W2 = 1.28$. It was selected due to be redder than typical quasars. This quasar exhibits broad absorption features blueward of the C IV and C III] emission lines, accompanied by significant suppression of the continuum in the rest-frame UV region (Fig. 6). The redshift is determined based on a prominent emission feature near 5230 Å, identified as C III] λ1909. This is consistent with the presence of Hα emission in the expected wavelength range in the SPHEREx spectrum. The SPHEREx spectrum is again contaminated by light from another source. There is no evidence of significant dust reddening ($A_V = 0$). The spectrum reveals prominent BAL characteristics. Therefore we label this object as a BAL quasar.

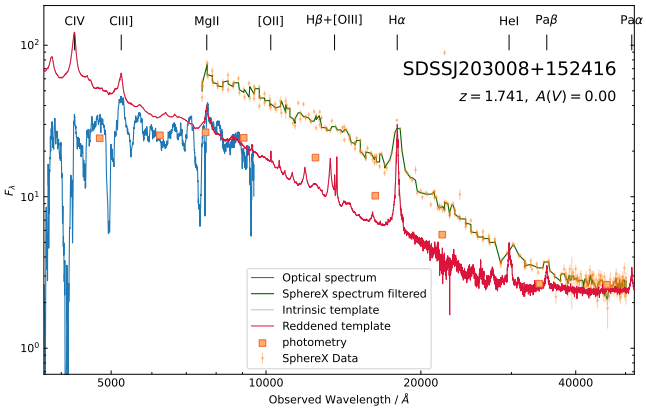


FIG. 6.— The spectrum of SDSS J203008+152416. We classify this source as a BAL quasar.

4.2.4. *SDSS J204757+002431 ($z = 1.850$)*

This object has colours $g - r = 1.33$, $J - K = 1.13$, and $W1 - W2 = 0.97$. It was selected due to its red optical colour. The redshift of this quasar is determined primarily from a set of strong absorption features, as its emission lines are significantly suppressed. In particular, Fe II λ2374, Fe II λ2382, Mn II λ2576, and Mn II λ2606 appear prominently in the observed spectrum. Consistent with $z = 1.850$, we also find that emission features such as C IV, C III] and Mg II align well with the template. The SPHEREx spectrum shows the presence of an Hα line consistent with this redshift. The spectrum exhibits several defining characteristics of a FeLoBAL quasar, including broad and blended absorption troughs, extensive low-ionization metal absorption (Fe II, Mn II, and Mg II) and continuum suppression over a wide wavelength range. The spectral shape is similar to the known FeLoBAL SDSS J090152.05+624342.6 (Wang et al. 2017). The position is covered by the FIRST survey, but no signal is detected from the source. We label this object as a FeLoBAL quasar.

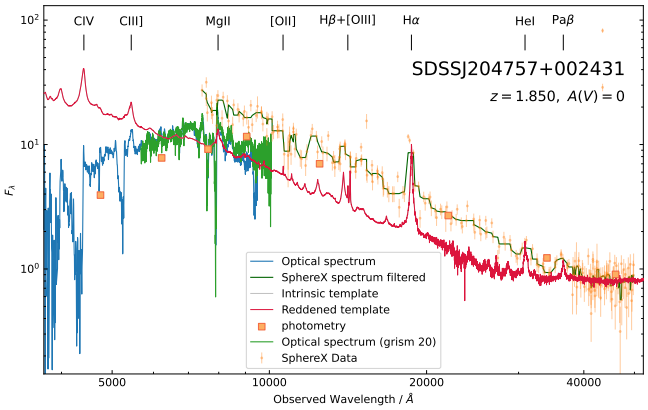


FIG. 7.— The spectrum of SDSS J204757+002031. We classify this source as a FeLoBAL quasar.

4.2.5. *SDSS J210215+230730 ($z = 0.139$)*

This object has colours $g - r = 0.97$, $J - K = 1.56$, and $W1 - W2 = 0.86$. It was selected for spectroscopic follow-up due to its red optical and near-infrared colours.

We determine a low redshift of 0.139 based on broad Hα and narrow [O II] and [O III] emission (see Fig. 8). Hβ and Mg II is also detected. The continuum is very red. In Fig. 8 we have not plotted the quasar template as it is not possible to match the spectrum with a quasar template reddened by SMC-like extinction. In SPHEREx the shape of the spectrum matches the photometry fairly well, but the photometry falls below the SPHEREx measurements, probably due to variability. The SPHEREx measurements are not contaminated by light from other sources. In SDSS the object is extended and is classified as a galaxy, but the $W1-W2$ colour is inconsistent with a galaxy (or stellar) spectrum. This is an object with contributions to the spectrum from both a central obscured AGN and from the underlying host galaxy, somewhat reminiscent of Little Red Dots at higher redshifts (LRDs, Matthee et al. 2024; Ronayne et al. 2026). The shape of the continuum is similar, but the Hα line does not have the exponential profile seen in LRD spectra. We classify it as a normal quasar/AGN due to its broad Hα line.

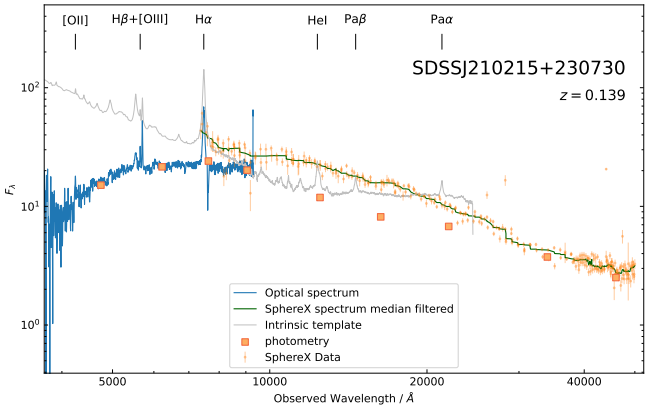


FIG. 8.— The spectrum of SDSS J210215+230730. We classify this source as a normal quasar. It is somewhat reminiscent of an LRD. This is the lowest redshift source in the sample. We do not overplot a reddened quasar template as it matches very poorly with any extinction.

4.2.6. *SDSS J210558+222457 (star)*

This object has colours $g-r=1.04$, $J-K=1.07$, and $W1-W2=-0.09$. It was selected due to its red optical and near-infrared colours and low $W1-W2$ colour suggesting it could be at high redshift. The spectrum of this object shows a distinctly stellar shape, lacking any broad emission lines characteristic of quasars. The spectrum is well matched by stars of spectral type K.

4.2.7. *SDSS J212319+254131 ($z=2.520$)*

This object has colours $g-r=0.94$, $J-K=1.07$ and $W1-W2=1.03$. It was selected due to its red optical colour. Similar to SDSSJ 194143+610107 and SDSSJ 204757+002431, this quasar exhibits no prominent emission features in the optical (see Fig. 10), making redshift determination in the optical relying on absorption lines. At $z=2.36$, a series of Fe II absorption features (e.g., λ2344, λ2374, λ2382) and low-ionization lines such as Mg II λ2796 λ2803. There is a also a

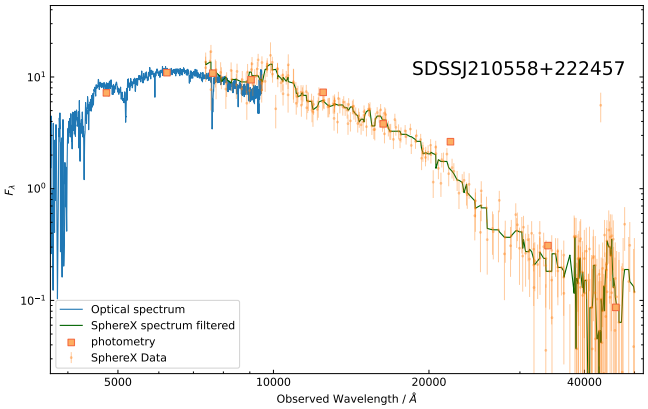


FIG. 9.— The spectrum of SDSS J210558+222457. We classify this source as a K-type star.

broad BAL-line in the blue end of the spectrum consistent with C IV at $z=2.36$. In the SPHEREx spectrum, however, the observed spectrum shows a prominent Hα emission feature, corresponding to a redshift of $z=2.52$ (Fig. 10). Taken together, this shows that this quasar is a high-velocity detached BAL quasar similar to the quasars studied by Fynbo et al. (2020) and Ma et al. (2026). It is however, unusual to see detached low-ionization lines.

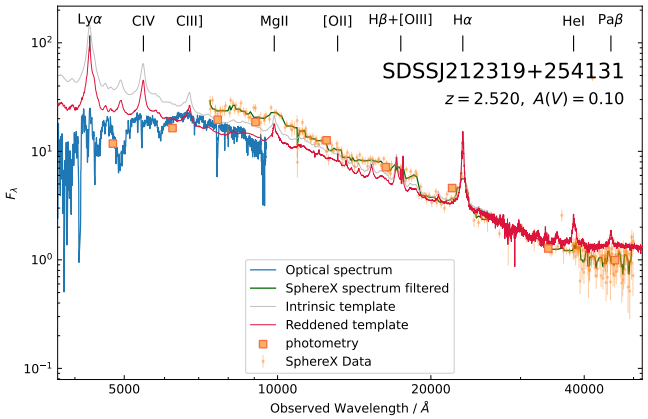


FIG. 10.— The spectrum of SDSS J212319+254131. We classify this source as a BAL quasar.

4.2.8. *SDSS J213510+272852 ($z=2.430$)*

This object has colours $g-r=1.06$, $J-K=1.78$, and $W1-W2=1.23$. It was selected for follow-up spectroscopy due to its red optical colour. The redshift of this quasar is determined based on the observed C III] emission feature, with supporting emission from Lyα and C IV clearly visible in the spectrum (see Fig. 11). There are clear BAL features bluewards of the C IV, Si IV and Lyα emission lines. In addition to the high-ionization features, absorption from the low-ionization Mg II doublet is present, allowing a further classification as a low-ionization BAL (LoBAL) quasar. A reddening value of $A_V=0.2$ provides an excellent match between the template and photometry. The source is detected by LOFAR with a flux of 6.27±0.41 mJy. We label this quasar as a LoBAL quasar.

4.2.9. *SDSS J214039+005705 ($z=1.156$)*

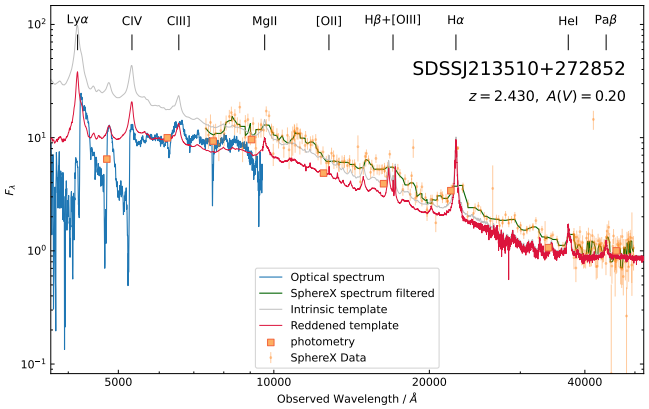


FIG. 11.— The spectrum of SDSS J213510+272852. We classify this source as a BAL quasar.

This object has colours $g-r=1.38$, $J-K=1.30$, and $W1-W2=1.36$. It was selected for follow-up spectroscopy due to its red optical colour. The redshift of this quasar is determined to be $z=1.1555$, based on the alignment of several prominent absorption features from Fe, Mn, and Mg (see Fig. 12). No strong emission lines are clearly identifiable in the optical. The continuum breaks blueward of Magnesium. In the SPHEREx spectrum there are emission lines from Hα, He I, and Paα consistent with $z=1.1555$. Over most of the spectra range a normal quasar template reddened by SMC-like extinction with $A_V=0.55$ gives a decent match, but below about 3000 Å the continuum seems to break. The position is covered by the FIRST survey, but no signal is detected from the source. We classify this source as a peculiar quasar.

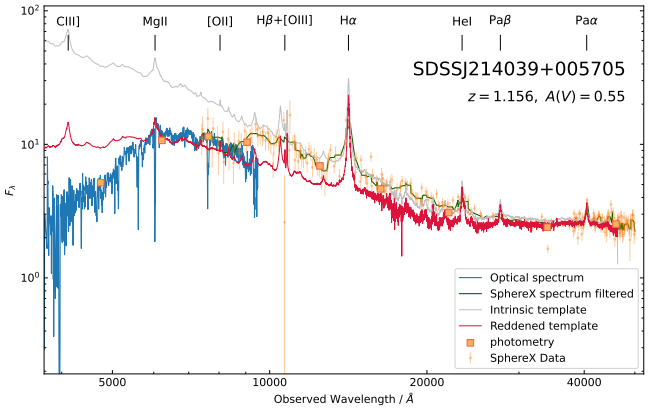


FIG. 12.— The spectrum of SDSS J214039+005705. We classify this source as a peculiar quasar.

4.2.10. *SDSS J215731+183120 ($z=2.020$)*

This object has colours $g-r=0.42$, $J-K=1.41$, and $W1-W2=1.09$. It was selected to have colours typical of a normal $z<2.8$ quasar. The redshift of this quasar is estimated to be $z=2.020$, primarily based on the alignment of prominent broad emission features in the optical including C III], C IV, and Lyα. The SPHEREx spectrum shows emission from Hα, Hβ, and Paβ. The extinction value $A_V=0.15$ provides a good match between the observed spectrum and the reddened template, indicating that the quasar is mildly reddened. The spectrum shows no clear signs of broad absorption troughs or strong low-ionization absorption lines. The source is detected by LOFAR with a flux of 2.57±0.10 mJy. Therefore, we classify SDSS J2157+183120 as a normal quasar.

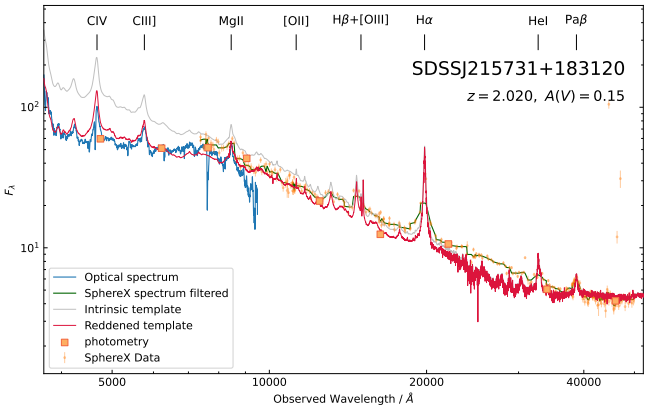


FIG. 13.— The spectrum of SDSS J215731+183120. We classify this source as a normal quasar.

4.2.11. *SDSS J215856+285434 ($z=1.553$)*

This object has colours $g-r=0.71$, $J-K=0.93$, and $W1-W2=1.20$. It was selected for follow-up spectroscopy due to its mildly red optical colour compared to normal quasars. The redshift of this quasar is estimated to be $z=1.553$ based on the identification of broad absorption features, including Fe II λ2344, λ2374, λ2382 and Mg IIλ2586, λ2600, λ2802 (see Fig. 14). The presence of strong, wide, and overlapping low-ionization absorption features—especially those from Fe II supports its classification as a low-ionization BAL quasar. Once the redshift is determined, we also find that the emission lines of C IV, C III], and Mg II align well with the template, although all are significantly suppressed. The SPHEREx spectrum is contaminated by light from a much brighter source. Despite of this, Paα emission is detected from the quasar at the expected wavelength.

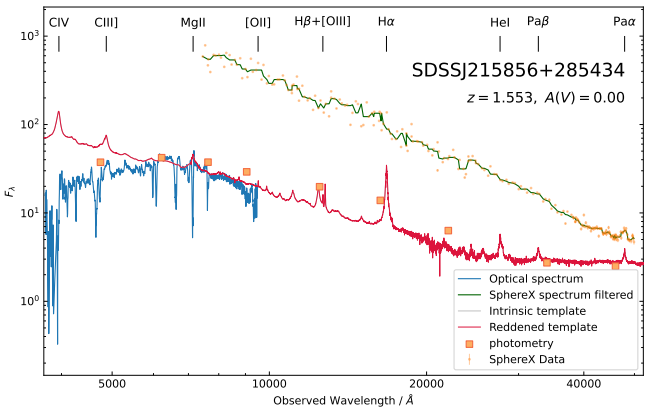


FIG. 14.— The spectrum of SDSS J215856+285434. We classify this source as a BAL quasar. The SPHEREx spectrum is blended with light from a brighter source.

4.2.12. *SDSS J221036+282050 ($z = 3.732$)*

This object has colours $g - r = 1.70$, $J - K = 1.21$, and $W1 - W2 = 0.27$. It was selected for follow-up spectroscopy due to its red optical colour and the low $W1 - W2$ colour, which could suggest a redshift larger than 2.8. We determine a redshift of $z = 3.732$ based on weak Lyα in the optical and Hα in the SPHEREx spectrum (see Fig. 15). The spectrum is well matched with a composite quasar spectrum mildly reddened ($A_V = 0.2$ mag). We classify this as a normal quasar.

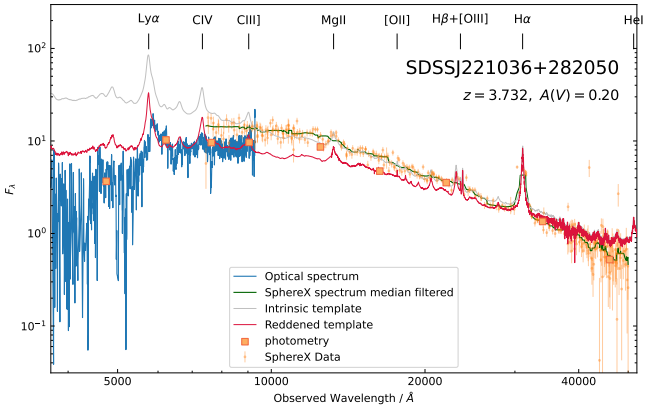


FIG. 15.— The spectrum of SDSS J221036+282050. We classify this source as a normal quasar. This is the highest redshift source in the sample.

4.2.13. *SDSS J222839+172759 ($z = 2.932$)*

This object has colours $g - r = 0.39$, $J - K = 1.37$, and $W1 - W2 = 0.78$. It was selected for follow-up spectroscopy due to its blue optical colour and red near-infrared colours. We determine a redshift of $z = 2.932$ based on Lyα and C III] in the optical and Hα in the SPHEREx spectrum. The spectrum is mildly reddened. There is a broad and detected BAL-feature from C IV. We categorize the source as a BAL quasar.

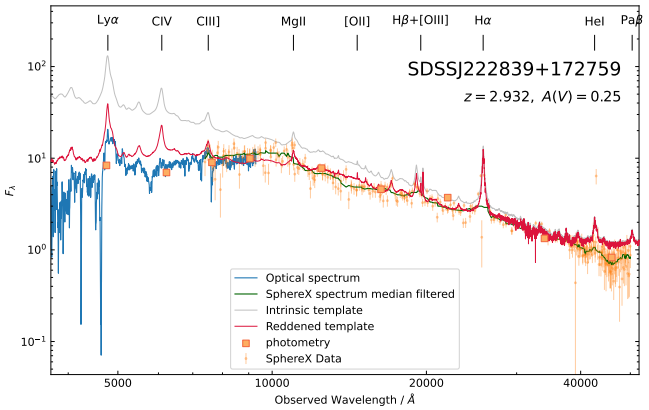


FIG. 16.— The spectrum of SDSS J222839+172759. We classify this source as a BAL quasar.

4.2.14. *SDSS J222934+101907 (star)*

This object has colours $g - r = 0.89$, $J - K = 1.13$, and $W1 - W2 = 0.52$. It was selected due to its red optical and near-infrared colours and borderline $W1 - W2$ colour. This object was determined not to be a quasar, based on the absence of any broad emission lines or high-redshift spectral features (see Fig. 17). We classify this target as a K-type star. The position is covered by the FIRST survey, but no signal is detected from the source as expected for a star.

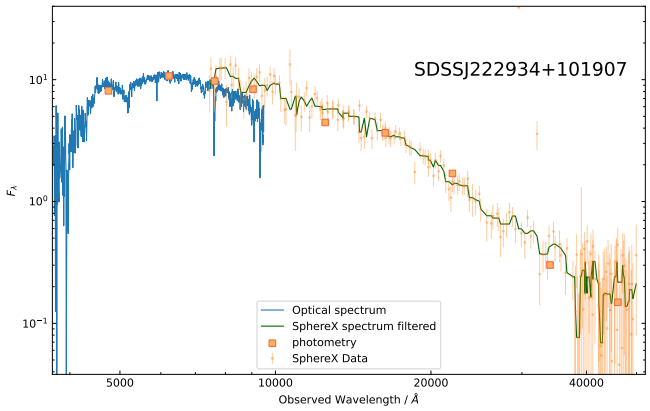


FIG. 17.— The spectrum of SDSS J222934+101907. We classify this source as K-type star.

4.2.15. *SDSS J223030+383246 ($z = 2.260$)*

This object has colours $g - r = 0.36$, $J - K = 1.44$, and $W1 - W2 = 1.08$. It was selected for follow-up spectroscopy to have colours typical of a normal $z < 2.8$ quasar. The redshift of this quasar is determined to be $z = 2.260$. The redshift is measured based on the C III] emission feature. Although the Lyα and C IV emission lines are also prominent, they are affected by associated absorption features and therefore are not suitable for Gaussian fitting. In the SPHEREx spectrum we see a prominent Hα line. With the help of photometric data, the extinction is determined to be $A_V = 0$. We classify this target as a normal quasar.

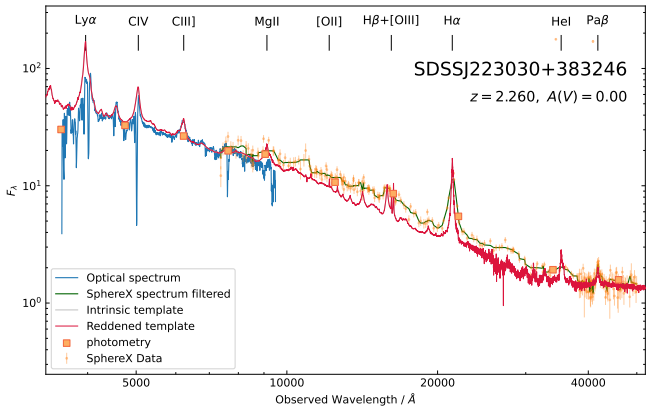


FIG. 18.— The spectrum of SDSS J223030+383246. We classify this source as a normal quasar.

4.2.16. *SDSS J225432+063826 ($z = 2.698$)*

This object has colours $g - r = 0.92$, $J - K = 1.24$, and $W1 - W2 = 1.06$. It was selected for follow-up spectroscopy due to its red colours. We determine a redshift

of 2.698 based on a mix of absorption (Lyα and C IV) and emission (C III]) features in the optical and emission lines (Hα and He I) in the SPHEREx spectrum. The spectrum is mildly reddened. We categorize the source as a peculiar quasar due to the weak emission lines in the restframe ultraviolet.

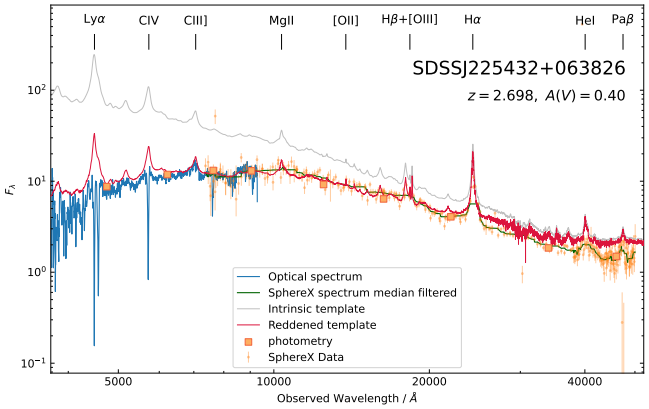


FIG. 19.— The spectrum of SDSS J225432+063826. We classify this source as a peculiar quasar.

4.2.17. *SDSS J231514+113820 ($z = 2.895$)*

This object has colours $g - r = 0.61$, $J - K = 0.85$, and $W1 - W2 = 1.11$. It was selected for follow-up spectroscopy due to its mildly red optical colour. This object is a classical BAL quasar (see Fig. 20. Its redshift ($z = 2.895$) is inferred from the Lyα and C IV emission features at the red edges of the BAL troughs. The SPHEREx spectrum shows emission lines from Hα and He I consistent with $z = 2.895$. The position is covered by the FIRST survey, but no signal is detected from the source.

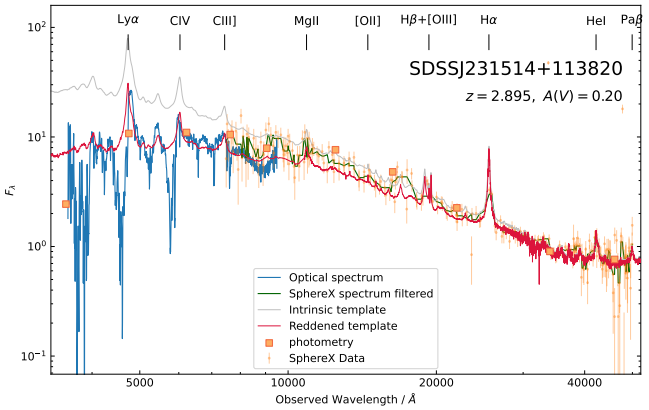


FIG. 20.— The spectrum of SDSS J231514+113820. We classify this source as a BAL quasar.

4.2.18. *SDSS J231704+160807 ($z = 0.464$)*

This object has colours $g - r = 1.32$, $J - K = 1.89$ and $W1 - W2 = 1.19$. It was selected for follow-up spectroscopy due to its very red optical colour. This object is a heavily reddened quasar at a fairly low redshift of $z = 0.464$ (see Fig. 21). Its redshift is determined based on the Hα emission feature round 9600 Å. The dust extinction is estimated to be $A_V = 1.7$, but the match is not very good, especially in the blue end of the optical range. There seems to be blueshifted absorption (by about 10^4 km s^{-1}) from both Hβ and Hα and possible also less blueshifted absorption from from He I. Also from Mg II there is blueshifted absorption. In the SPHEREx spectrum we see Hα, He I, and Paschen lines. We label the object as a peculiar quasar.

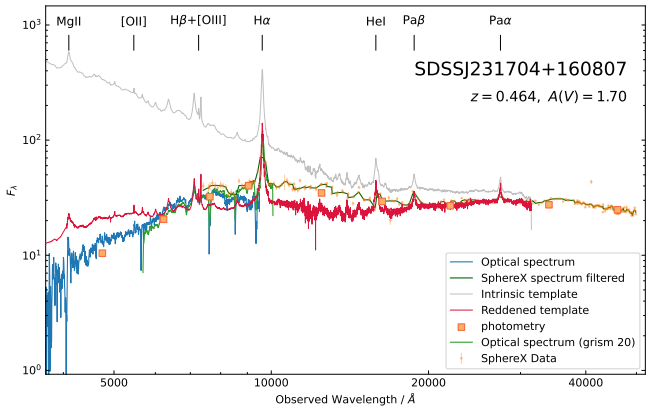


FIG. 21.— The spectrum of SDSS J231704+160807. We classify this source as a peculiar quasar.

4.2.19. *SDSS J231817+234950 ($z = 0.570$)*

This object has colours $g - r = 0.76$, $J - K = 1.69$, and $W1 - W2 = 1.08$. it was selected for follow-up spectroscopy due to its red optical colours. We determine a redshift of $z = 0.570$ based on a range of features in the optical and SPHEREx spectra (see Fig. 22. The spectrum is fairly well represented by a reddened template with $A_V = 1.50$. We classify this source as a normal, reddened quasar.

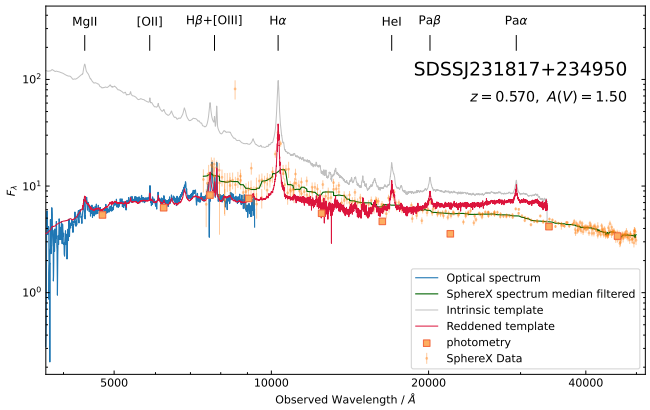


FIG. 22.— The spectrum of SDSS J231817+234950. We classify this source as a normal, reddened quasar.

4.2.20. *SDSS J232521+191557 (star)*

This object has colours $g - r = 1.51$, $J - K = 1.17$, and $W1 - W2 = 0.22$. It was selected due to its red optical colour. The spectrum of this object lacks the broad emission lines typically observed in quasars (see Fig. 23). We

identify several key features commonly associated with M-type stars, such as strong TiO absorption bands that shape the overall shape of the spectrum. We classify this target as an M-type star.

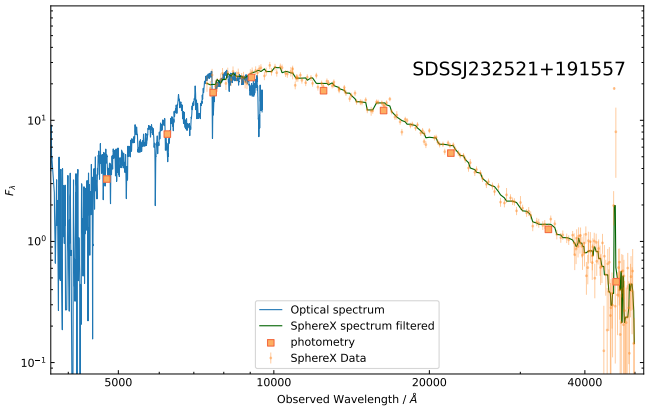


FIG. 23.— The spectrum of SDSS J232521+191557. We classify this source as an M-type star.

4.2.21. *SDSS J233334+291822 ($z = 1.675$)*

This object has colours $g - r = 1.36$, $J - K = 1.09$, and $W1 - W2 = 0.92$. The object was selected for spectroscopy due to its red optical colours. The spectrum has a single weak emission line in the restframe ultraviolet, namely C III]. There is a BAL line at the position of C IV. In the SPHEREx spectrum we detect Hα. The spectrum is reddened, but the reddened template does not match the observed spectrum well bluewards of Mg II. We classify the object as a BAL quasar.

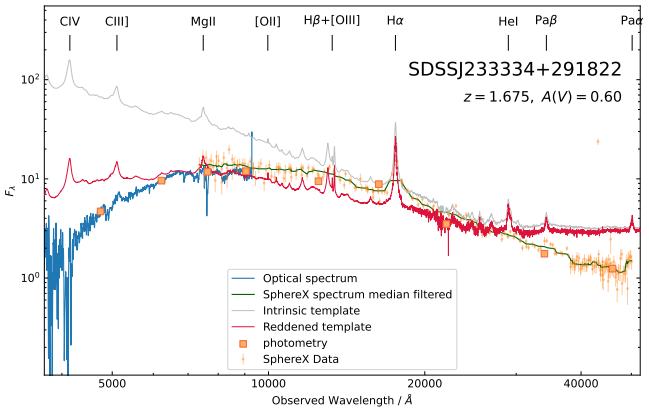


FIG. 24.— The spectrum of SDSS J233334+291822. We classify this source as a BAL quasar.

4.2.22. *SDSS J234610+431950 ($z = 3.260$)*

This object has colours $g - r = 0.42$ and $W1 - W2 = 0.75$. It was selected for follow-up spectroscopy due to its borderline $W1 - W2$ colour suggesting it could be a quasar at $z > 2.8$. This target is indeed a quasar at a relatively high redshift of $z = 3.260$ (see Fig. 25). The redshift is calculated based on the prominent emission lines from Lyα and C IV. In the SPHEREx spectrum we also detect a prominent Hα emission line. We classify it as a normal quasar.

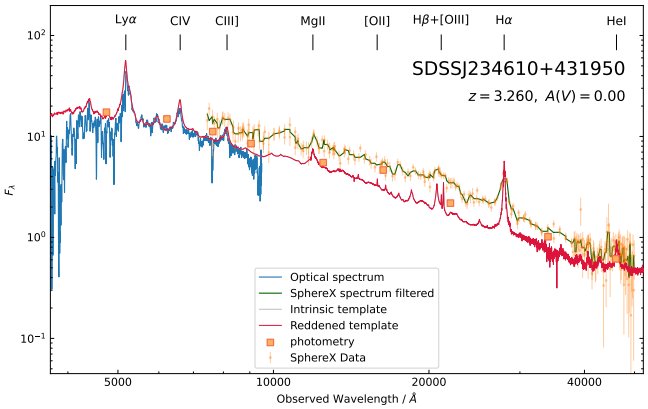


FIG. 25.— The spectrum of SDSS J234610+431950. We classify this source as a normal quasar.

4.2.23. *SDSS J234703+373435 ($z = 3.030$)*

This object has colours $g - r = 0.49$, $J - K = 1.46$, and $W1 - W2 = 1.00$. It was selected to be a normal quasar. This object is a quasar with a fairly high redshift $z = 3.030$ (see Fig. 26). The redshift is determined based on the Lyα and C IV emission lines. In the SPHEREx spectrum we detect bright emission lines consistent with Hα and He I at this redshift. The dust extinction is estimated to be $A_V = 0.20$. The source is detected by LOFAR with a flux of 1.28±0.09 mJy.

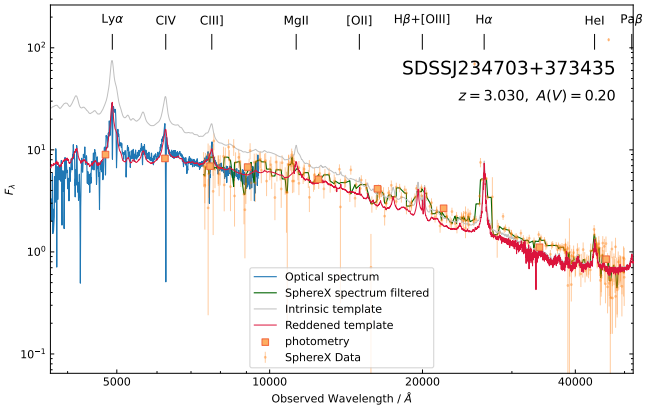


FIG. 26.— The spectrum of SDSS J234703+373435. We classify this source as a normal quasar.

4.2.24. *SDSS J235003+241943 ($z = 0.692$)*

This object has colours $g-r = 0.83$, $J-K = 1.30$, and $W1 - W2 = 1.06$. The object was selected for follow-up spectroscopy due to its red optical colour. We determine a redshift of $z = 0.692$ based on Hβ and [O III] emission the optical and Hα in the SPHEREx spectrum. There is no line emission from Mg II. The shape of the spectrum is poorly matched by a reddened quasar template. We categorize the object as a peculiar quasar.

4.3. *The confirmed quasars*

The 21 confirmed quasars span a wide redshift range from $z = 0.139$ to $z = 3.732$. The estimated dust extinction values cover a range of $A_V = 0$ to $A_V = 1.7$. As expected, the most dust obscured objects are at the lowest redshifts as shown in Fig. 28. This is what we expect

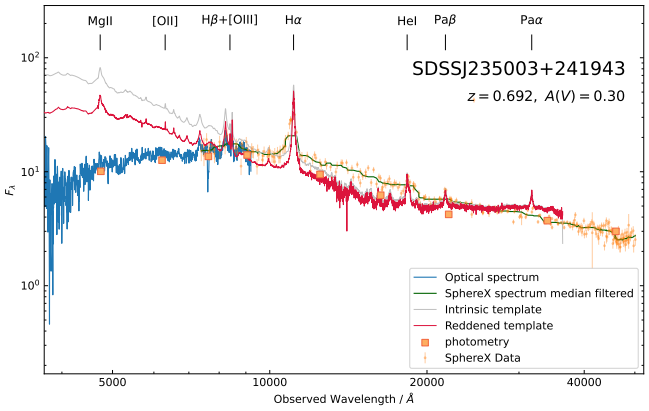


FIG. 27.— The spectrum of SDSS J235003+241943. We classify this source as a peculiar quasar.

due to Malmquist bias and due to the fact that it requires higher extinction to redden a spectrum in the observed optical range for a lower redshift source compared to a higher redshift source.

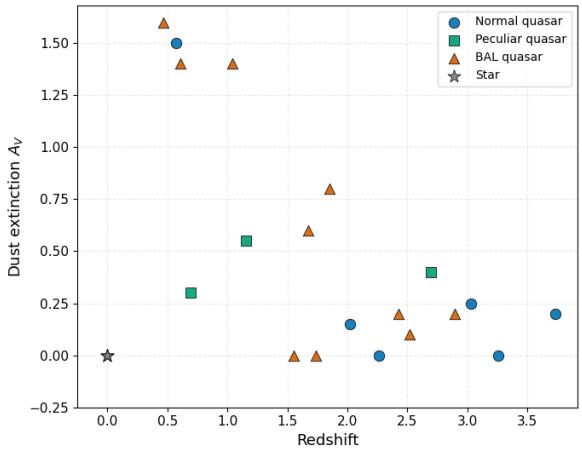


FIG. 28.— Estimated dust extinction, A_V, as a function of redshift for the confirmed quasars. Different marker shapes indicate the spectral classifications of the quasars. The most highly extinguished objects are found predominantly at relatively low redshifts.

Based on their spectral characteristics, the confirmed quasars are classified into 7 normal quasars (including some that are obscured) and 11 broad absorption line (BAL) quasars, and three peculiar quasars with very weak emission lines. Among the BAL quasars, four objects are further classified as FeLoBAL quasars, identified by the presence of strong Fe II absorption features in their spectra.

Fig.2 shows the distribution of all observed candidates in the $g-r$ versus $J-K$ colour-colour diagram. The quasars occupy a broad region of the colour-colour space, extending beyond the main locus of optically selected quasars. BAL quasars are predominantly located at higher $g-r$ values, occupying the upper part of the diagram. In contrast, the normal quasars cluster toward lower $g-r$ values, close to the region typically populated by optically selected quasars.

4.4. *Stars*

Among the 17 spectroscopically observed candidates, three objects are classified as late-type stars (stellar class K and M). These stars are located close to the boundary between the quasar and stellar loci in the $g-r$ versus $J-K$ colour–colour diagram, consistent with their spectroscopic identification.

5. DISCUSSION

5.1. *Theoretical and empirical structure of the colour–colour diagram*

As discussed in Sect. 2.2, the theoretical colour tracks in the $g-r$ vs. $J-K$ diagram derived from spectral templates predict a relatively narrow stellar locus, a lower quasar locus, and intermediate regions in which the two populations approach or overlap. These predictions formed the basis for the division of sources into relatively clean stellar and quasar regions and more ambiguous regions with significant overlap of sources of different nature.

The distribution of the full zero-proper-motion sample in Fig. 29 provides an empirical test of this interpretation. Sources with $W1-W2 \leq 0.8$ form a comparatively narrow, vertically extended sequence that broadly follows the predicted stellar locus. There is also a clear overdensity of points at the position expected for galaxies at around $J-K=1.0$ and $g-r=0.8$. In contrast, sources satisfying the commonly used mid-infrared AGN selection criterion, $W1-W2>0.8$, based on the criterion proposed by Stern et al. (2012), are concentrated mainly in the lower (in $g-r$) and redder (in $J-K$) parts of the diagram, close to the regions occupied by the theoretical quasar tracks. The broad correspondence between the optical–near-infrared colour structure and the independent mid-infrared criterion therefore supports the main features predicted by the templates.

However, the separation is not complete. Sources on both sides of the $W1-W2=0.8$ threshold are present in the central and transitional parts of the diagram. The overlap is especially apparent in the regions where the stellar sequence approaches the blue and average quasar tracks, and where the red quasar tracks extend towards colours also occupied by stars, as shown by the theoretical colour tracks in Fig. 2. Thus, neither the position in the $g-r$ versus $J-K$ diagram nor the $W1-W2$ criterion alone provides an unambiguous classification throughout the full colour space.

The comparison shows that some regions of the colour–colour diagram provide a more reliable separation between stars and quasars than others. The relatively blue $J-K$ part of the stellar sequence remains dominated by sources with $W1-W2 \leq 0.8$, consistent with its interpretation as a comparatively clean stellar region. Similarly, the lower quasar locus contains a high concentration of sources with $W1-W2>0.8$ and can therefore be regarded as a relatively clean quasar region. Between these areas, the presence of both mid-infrared populations indicates that the transitional regions are more difficult to classify using photometric colours alone.

These results show that the theoretical tracks provide a useful first-order description of the source distribution, while the mid-infrared information offers an independent but imperfect empirical discriminator. Their combination identifies regions in which photometric classification

is relatively reliable, as well as regions in which spectroscopic follow-up remains essential.

The spectroscopic classifications of the selected targets provide a more direct test of these regional interpretations and reveal a particularly notable difference between quasars found in the clean and transitional parts of the diagram.

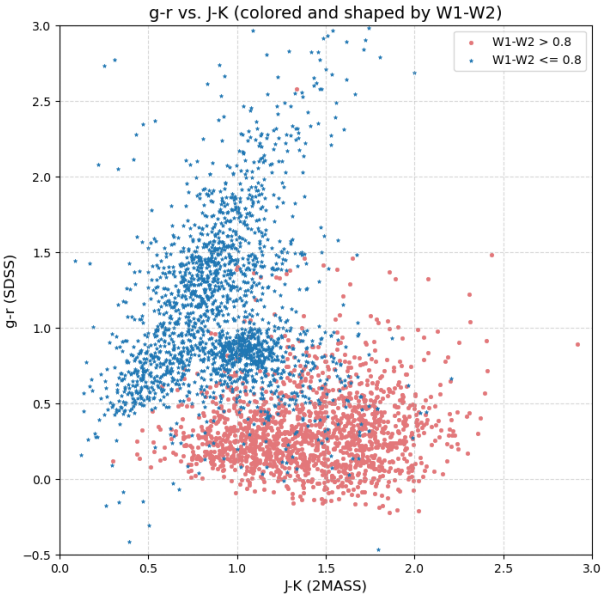


FIG. 29.— The $g-r$ versus $J-K$ color–color diagram of objects selected from astrometric pre-selection. Objects with $W1-W2 > 0.8$ (typically associated with quasars or AGNs) are shown as red circles, while those with $W1-W2 \leq 0.8$ (likely stars and galaxies) are shown in blue.

5.2. *BAL quasars and peculiar quasars in the overlapping colour regions*

Figure 30 shows the positions of the observed targets in the $g-r$ versus $J-K$ and $W1-W2$ versus $J-K$ diagrams, with marker shapes indicating their spectroscopic classifications. The quasars are coloured by redshift in the left panels and by the estimated dust extinction, A_V, in the right panels.

The spectroscopic classifications are broadly consistent with the expectations in the relatively well-separated regions of the colour–colour diagram. The single target observed in the star-safe region was confirmed to be a star, while all three targets located in the lower part of the traditional quasar-safe region in the $g-r$ versus $J-K$ diagram were confirmed as normal quasars. In contrast, the targets selected from the transitional regions show much more diverse classifications, including stars, normal quasars, BAL quasars, and peculiar quasars. Strikingly, only two of the 15 quasars confirmed in these more ambiguous regions are normal quasars. All BAL and peculiar quasars in our sample are located within these transitional regions.

No simple redshift sequence is apparent in either colour–colour plane. Quasars over a broad range of redshifts occupy overlapping regions, while objects at similar redshifts can have substantially different colours. The displacement of BAL and peculiar quasars from the normal-quasar locus therefore cannot be explained by redshift alone. The panels coloured by A_V show that some of the reddest objects have relatively high estimated extinctions, suggesting that dust reddening contributes to their positions.

However, the relation between A_V and broad-band colour is not one-to-one: quasars with comparable extinction values may occupy different parts of the diagrams, and some objects with low fitted extinction also show unusual colours. The explanation for this distribution is the complexity of the spectral features of the BAL and peculiar quasars. For BAL quasars, their broad line absorption features can suppress the flux of one or more photometric bands and therefore alter the observed broad band colours. This effect may shift some BAL quasars away from the relatively clean quasar region into the overlapping or transition parts of the colour–colour diagram.

The peculiar quasars in our sample do not share a single spectral characteristic that can explain their locations in the colour–colour diagrams. Instead, they exhibit a variety of departures from normal quasar spectra. These include a pronounced continuum break blueward of Mg II in SDSS J214039+005705, unusually weak rest-frame ultraviolet emission lines in SDSS J225432+063826, and the absence of prominent Mg II emission together with a continuum poorly reproduced by a reddened quasar template in SDSS J235003+241943. Such variations in continuum shape and emission-line strength can affect the flux measured in individual photometric bands, producing unusual broad-band colours even when the fitted dust extinction is modest. The locations of the peculiar quasars therefore likely reflect their heterogeneous spectral properties rather than a single effect such as redshift or dust reddening.

The distribution of the BAL quasars and the peculiar quasars in the photometrically ambiguous regions demonstrates the value of deliberately sampling outside the clean quasar locus. Selection methods optimized for high purity may avoid this regions because of their stronger stellar contamination, but may consequently miss quasars with complex spectral properties. The result of this work suggests that BAL quasars may occur at a relatively higher frequency than in the relatively clean quasar region. However, the present sample is small and was not selected to be statistically representative, so a larger sample is required to test this possibility.

5.3. *Unusual extinction properties in two low-redshift BAL quasars*

Among the BAL quasars in our sample, two objects, SDSS J182859+643725 and SDSS J231704+160807, exhibit spectral properties that are particularly unusual. In both cases, the observed flux at short wavelength falls systematically below the best fitting reddened quasar template. The SMC-like extinction curve cannot simultaneously reproduce the longer wavelength continuum and the suppression towards the blue.

Part of this discrepancy may be related to the broad absorption features themselves. However, the strongest absorption features in these two spectra are mainly located at longer observed wavelengths, as shown in Fig. 31, whereas the shorter-wavelength continuum is systematically suppressed relative to the reddened template without comparably prominent absorption fea-

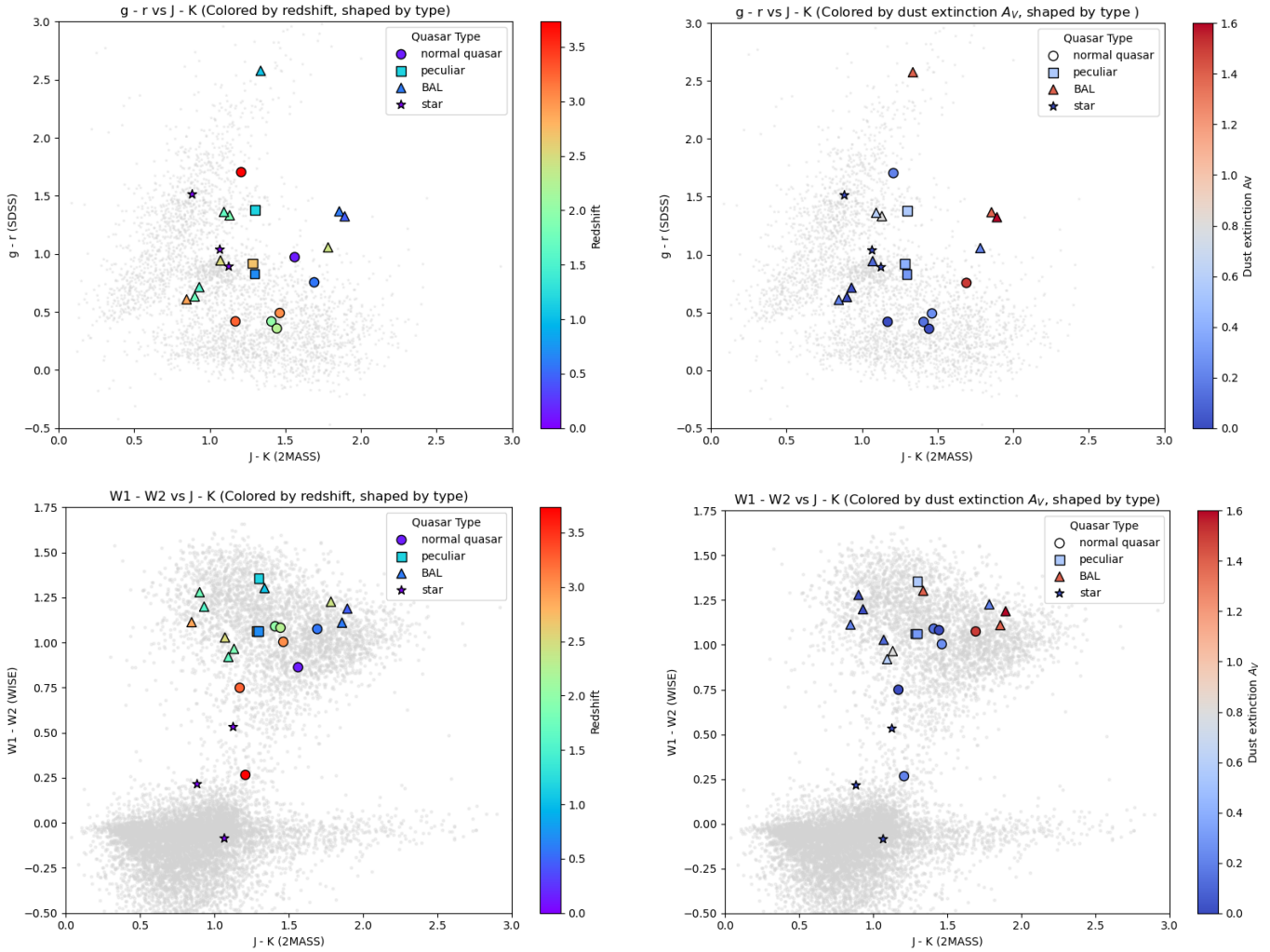


FIG. 30.— Colour–colour diagrams showing the locations of the spectroscopically observed targets. The top panels show $g-r$ versus $J-K$, while the bottom panels show $W1-W2$ versus $J-K$. Marker shapes indicate the spectroscopic classifications of the targets. In the left panels, quasars are coloured according to their redshifts, while in the right panels they are coloured according to their estimated dust extinctions, A_V. Grey background points represent objects in the full zero-proper-motion sample. Stars are shown using a fixed colour, since redshift and quasar extinction estimates are not applicable to them.

tures. Their absorption features are located blueward of Balmer and Helium lines, which is unusual for BAL quasars (Leighly et al. 2025).

One possible explanation is that the dust extinction towards these quasars differs from the SMC-like law adopted in the fitting. A steeper extinction curve would produce stronger attenuation at short wavelengths while leaving the longer-wavelength continuum comparatively less affected, and could therefore provide a better qualitative description of the observed spectral shape. A similarly steep extinction law has previously been suggested for reddened quasars for which an SMC-like curve could not reproduce both the optical spectra and the near-infrared photometry (Fynbo et al. 2013). Such a steep extinction curve may, in principle, be associated with a dust-grain population weighted towards smaller grains, which absorb and scatter short-wavelength radiation more efficiently.

5.4. *SPHEREx*

Finally we note that SPHEREx spectra are extremely useful for this kind of work as they provide extra features for redshift determination. In some case this was crucial for identifying the correct redshift (e.g., the case of SDSS J212319+254131).

6. CONCLUSIONS AND OUTLOOK

We investigated 24 quasar candidates selected using Gaia astrometry and multi-wavelength photometry, with targets sampled from both relatively clean and transitional regions of the $g-r$ versus $J-K$ colour–colour diagram. Spectroscopic observations confirm 21 quasars and three stars. The quasars span $z = 0.139$–3.732 and have estimated extinction values of $A_V = 0$–1.7. Seven are classified as normal quasars (one of which is reminiscent of an LRD), 11 as BAL quasars, and three as peculiar quasars with weak emission lines.

The classifications in the relatively clean regions agree with the theoretical expectations: the single target selected from the stellar region was confirmed as a star, while all four targets selected from the safe quasar region were confirmed as normal quasars. In contrast, the transitional regions contain both stars and quasars, and all ten quasars confirmed there are BAL quasars. This

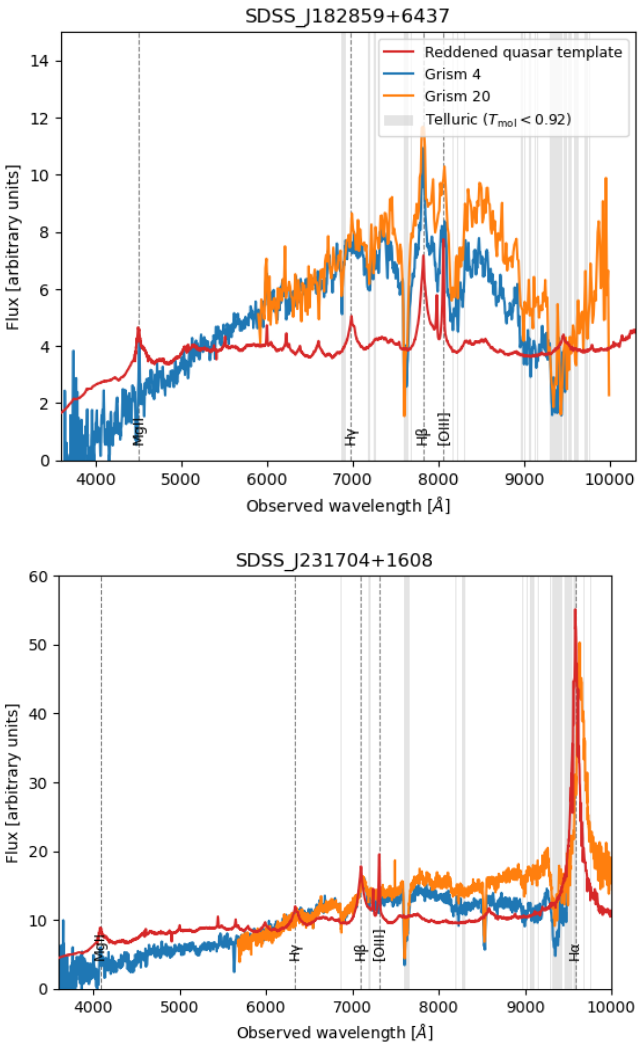


FIG. 31.— Observed spectra of SDSS J182859+643725 (top) and SDSS J231704+160807 (bottom), compared with their best-fitting reddened quasar templates. The blue and orange curves show the spectra obtained with ALFOSC Grism 4 and Grism 20, respectively, while the red curves represent the best-fitting reddened quasar templates scaled as in Fig. 4 and Fig. 21, respectively. The vertical dashed lines indicate the expected observed wavelengths of the labeled spectral features. The grey shaded regions mark wavelength intervals affected by telluric absorption, where the atmospheric transmission is below 0.92. In both objects, the observed continua fall systematically below the templates at short wavelengths, whereas the most prominent absorption troughs occur mainly at longer observed wavelengths. In particular, the similar mismatch at the blue end of both spectra cannot readily be explained by the prominent absorption troughs alone and may indicate an extinction curve steeper than the SMC-like curve adopted in the fitting.

suggests that BAL quasars may occur more frequently in photometrically ambiguous regions, although a larger and more systematic sample is required to test this possibility.

The addition of near-infrared spectra from SPHEREx was particularly useful in confirming redshifts when optical spectra were complex or difficult to interpret, including SDSS J182859+643725, SDSS J194143+610107, SDSS J212319+254131 and SDSS J214039+005705.

[4] https://www.astropy.org

Two BAL quasars also show unusually suppressed blue continua that cannot be reproduced well by the adopted SMC-like reddened template. A steeper extinction curve may provide a possible explanation.

Overall, our results show that combining astrometric selection, colour–colour sampling, and optical and near-infrared spectroscopy is effective for identifying quasars with unusual absorption and reddening properties.

Starting this year, the Purely Astrometric Quasar Survey (PAQS, Krogager et al. 2023) will start building up a sample of of order 300.000 sources selected from Gaia astrometry down to a Gaia G magnitude limit of 20.5 and followed up spectroscopically with the 4MOST instrument in Chile. This survey will sample the whole colour space (including the position of the stellar track) and will hopefully give us a clean census of the quasar population down to the survey flux limit.

ACKNOWLEDGEMENTS

We thank Tom Reynolds for helpful advice about SPHEREx spectra and for helpful discussions about the interpretation of several of the spectra. We thank Pascal Oesch for helpful discussions concerning LRDs. This work made use of Astropy[4]: a community-developed core Python package and an ecosystem of tools and resources for astronomy (Astropy Collaboration et al. 2022).

FUNDING: The Cosmic Dawn Center (DAWN) is funded by the Danish National Research Foundation under grant DNRF140. JPUF is supported by the Independent Research Fund Denmark (DFF-4090-00079) and thanks the Carlsberg Foundation for support. JPUF acknowledges support by the European Research Council (ERC) under the European Union's research and innovation program (ERC Grant HEAVYMETAL No. 101071865).

DATA AND MATERIALS AVAILABILITY: Based on observations made with the Nordic Optical Telescope, installed in the Spanish Observatorio del Roque de los Muchachos of the Instituto de Astrofísica de Canarias. The data presented here were obtained in part with ALFOSC, which is provided by the Instituto de Astrofisica de Andalucia (IAA) under a joint agreement with the University of Copenhagen and NOT. The NOT data were obtained under program 69-802. This work has made use of data from the European Space Agency (ESA) mission Gaia, processed by the Gaia Data Processing and Analysis Consortium (DPAC). Funding for the DPAC has been provided by national institutions, in particular the institutions participating in the Gaia Multilateral Agreement. This publication makes use of data products from the Spectro-Photometer for the History of the Universe, Epoch of Reionization and Ices Explorer (SPHEREx), which is a joint project of the Jet Propulsion Laboratory and the California Institute of Technology, and is funded by the National Aeronautics and Space Administration.

REFERENCES

Alam, S., Albareti, F. D., Allende Prieto, C., et al. 2015, ApJS, 219, 12, doi: 10.1088/0067-0049/219/1/12
Assef, R. J., Kochanek, C. S., Brodwin, M., et al. 2010, ApJ, 713, 970, doi: 10.1088/0004-637X/713/2/970
Astropy Collaboration, Price-Whelan, A. M., Lim, P. L., et al. 2022, ApJ, 935, 167, doi: 10.3847/1538-4357/ac7c74
Bock, J. J., Aboobaker, A. M., Adamo, J., et al. 2026, ApJ, 999, 139, doi: 10.3847/1538-4357/ae2be2
de Gasperin, F., Edler, H. W., Williams, W. L., et al. 2023, A&A, 673, A165, doi: 10.1051/0004-6361/202245389
Fan, X. 2006, New Astronomy Reviews, 50, 665
Fynbo, J. P. U., Krogager, J.-K., Venemans, B., et al. 2013, ApJS, 204, 6, doi: 10.1088/0067-0049/204/1/6
Fynbo, J. P. U., Krogager, J.-K., Heintz, K. E., et al. 2017, A&A, 606, A13, doi: 10.1051/0004-6361/201730726
Fynbo, J. P. U., Møller, P., Heintz, K. E., et al. 2020, A&A, 634, A111, doi: 10.1051/0004-6361/201936957
Gaia Collaboration, Prusti, T., de Bruijne, J. H. J., et al. 2016, A&A, 595, A1, doi: 10.1051/0004-6361/201629272
Geier, S. J., Heintz, K. E., Fynbo, J. P. U., et al. 2019, A&A, 625, L9, doi: 10.1051/0004-6361/201935108
Gibson, R. R., Jiang, L., Brandt, W. N., et al. 2009, ApJ, 692, 758, doi: 10.1088/0004-637X/692/1/758
Heintz, K. E., Fynbo, J. P. U., & Høg, E. 2015, A&A, 578, A91, doi: 10.1051/0004-6361/201526038
Heintz, K. E., Fynbo, J. P. U., Høg, E., et al. 2018, A&A, 615, L8, doi: 10.1051/0004-6361/201833396
Heintz, K. E., Fynbo, J. P. U., Geier, S. J., et al. 2020, A&A, 644, A17, doi: 10.1051/0004-6361/202039262
Helfand, D. J., White, R. L., & Becker, R. H. 2015, ApJ, 801, 26, doi: 10.1088/0004-637X/801/1/26
Hewett, P. C., Warren, S. J., Leggett, S. K., & Hodgkin, S. T. 2006, MNRAS, 367, 454, doi: 10.1111/j.1365-2966.2005.09969.x
Hopkins, P. F., Somerville, R. S., Hernquist, L., et al. 2006, The Astrophysical Journal, 652, 864
Husser, T.-O., Wende-von Berg, S., Dreizler, S., et al. 2013, A&A, 553, A6, doi: 10.1051/0004-6361/201219058
Koo, D. C., Kron, R. G., & Cudworth, K. M. 1986, PASP, 98, 285, doi: 10.1086/131756
Krogager, J.-K., Leighly, K. M., Fynbo, J. P. U., et al. 2023, The Messenger, 190, 38, doi: 10.18727/0722-6691/5310
Leighly, K. M., Gallagher, S. C., Choi, H., et al. 2025, ApJ, 993, 129, doi: 10.3847/1538-4357/ae04df
Ma, G., Geier, S. J., Fynbo, J. P. U., et al. 2026, arXiv e-prints, arXiv:2607.01330, doi: 10.48550/arXiv.2607.01330
Matthee, J., Naidu, R. P., Brammer, G., et al. 2024, ApJ, 963, 129, doi: 10.3847/1538-4357/ad2345
Meiksin, A. A. 2009, Reviews of Modern Physics, 81, 1405
Meusinger, H., Scholz, R.-D., Irwin, M., & Lehmann, H. 2002, A&A, 392, 851, doi: 10.1051/0004-6361:20021014
Pei, Y. C. 1992, ApJ, 395, 130, doi: 10.1086/171637
Rees, M. J. 1984, Annual Review of Astronomy and Astrophysics, 22, 471
Ronayne, K., Papovich, C., Kirkpatrick, A., et al. 2026, ApJ, 1003, 234, doi: 10.3847/1538-4357/ae5e6b
Sandage, A. 1965, ApJ, 141, 1560, doi: 10.1086/148245
Schmidt, M. 1963, Nature, 197, 1040, doi: 10.1038/1971040a0
Selsing, J., Fynbo, J. P. U., Christensen, L., & Krogager, J. K. 2016, A&A, 585, A87, doi: 10.1051/0004-6361/201527096
Skrutskie, M. F., Cutri, R. M., Stiening, R., et al. 2006, AJ, 131, 1163, doi: 10.1086/498708
Stern, D., Assef, R. J., Benford, D. J., et al. 2012, ApJ, 753, 30, doi: 10.1088/0004-637X/753/1/30
Valeckas, K., Fynbo, J., Krogager, J.-K., & Heintz, K. 2025, The Journal of Open Source Software, 10, 9264, doi: 10.21105/joss.09264
Wang, J., Xu, D., & Wei, J. 2017, Frontiers in Astronomy and Space Sciences, 4, 40, doi: 10.3389/fspas.2017.00040
Wright, E. L., Eisenhardt, P. R. M., Mainzer, A. K., et al. 2010, AJ, 140, 1868, doi: 10.1088/0004-6256/140/6/1868

This paper was built using the Open Journal of Astrophysics LaTeX template. The OJA is a journal which provides fast and easy peer review for new papers in the astro-ph section of the arXiv, making the reviewing process simpler for authors and referees alike. Learn more at http://astro.theoj.org.